International Research Journal of Environmental Sciences ISSN 2319–1414
Vol. **14(3),** 50-73, July **(2025)** *Int. Res. J. Environmental Sci.*

Simulation of Gaseous Species and their Sensitivity towards the Regional Emission Inventory over Delhi, India using the Polyphemus modeling System

Saurabh Kumar[1,2*]
[1]Department of Mathematics, Braj Mohan Das College, Dayalpur, Babasaheb Bhimrao Ambedkar Bihar University, Muzaffarpur, Bihar, India
[2]Centre for Atmospheric Sciences, Indian Institute of Technology Delhi, New Delhi, India
skumarcas@gmail.com

Available online at: www.isca.in, www.isca.me
Received 2nd January 2025, revised 12th April 2025, accepted 24th June 2025

Abstract

Air quality models are invaluable instruments for estimating and analyzing the concentration of air pollutants in the atmosphere. This paper evaluates the impact of regional emission inventory and global inventory EDGAR through the simulated air quality. The present study utilized the Polyphemus chemical transport model (CTM) over Delhi, India to simulate various chemical species. In particular, the impact of regional emission inventory on the simulations of gaseous species like Ozone (O_3), Nitrogen dioxide (NO_2), Nitrous oxide (NO), Carbon monoxide (CO) and Sulphur dioxide (SO_2) are analyzed over the national capital of India. In order to analyse the impact of regional emission data on simulated gaseous species diurnal variation, time-series plots and statistical metrics are analyzed at multiple monitoring stations situated in the simulation domain. Regional emission inventory prepared for the base year 2010, takes into account of various sectors such as Industry, Road Transport, Waste disposal and Burning, Brick Kilns, vehicles etc. Anthropogenic impact on gaseous species as NO, NO_2, CO and SO_2concentration levels are observed. EDGAR global inventory for the base year 2010 is also used to analyze the comparative performance of megacity regional inventory. The ground level modelled concentration of O_3, NO, NO_2, CO and SO_2 are compared with the monitored value at various locations. A regional emission inventory is able to capture NO, NO_2 and CO concentration, whereas O_3 is better predicted with EDGAR. The impact of the emission reduction scenario of major precursors NO_X and VOCs on simulated O_3 concentration has been analyzed. It will expedite the model response towards the emission changes that can be conducive to policy support also.

Keywords: Emission inventory, Chemistry-Transport Model, Ozone, Chemical mechanism, CB05.

Introduction

Rapid Urbanization and unprecedented growth have been two important factors generally responsible for the degradation in the air quality of megacities. Apart from anthropogenic emission sources located in urban areas, atmospheric dispersion and transport play a very crucial and significant role in creating pollution episodes. Delhi, the National Capital of India, home land of over 30 million residences in the year 2020 (https://populationstat.com/india/). In South Asia, it is among the economic hubs with the quickest rate of growth and has experienced unprecedented expansion in all domains including housing, transportation and industry during the last two decades[1]. This economic boom has resulted in deteriorating the air quality of the national capital region Delhi. Delhi, encompassing about 900 Square Km, the deteriorated air quality issue has detrimental consequences on human health. Various air pollution sources in Delhi range from road transport, industrial activities, domestic and waste burning. Gurjar and team have pointed out that the transport sector contributed more than 80% of nitrogen oxides (NO_X), carbon monoxide (CO) and volatile organic compounds (VOCs) towards pollution of Delhi[2]. Kansal et al. (2011) estimated that vehicles contribute about 90% of nitrogen dioxide (NO_2) towards air pollution[3]. In addition to it, Sahu and team estimated an increase of nearly 69% in NOx emissions over India from 2000 to 2011[4]. Several scientific studies have concluded that the air pollution in Delhi has resulted in a severe impact on human health ranging from cardiovascular, skin diseases, and respiratory illnesses to death[5]. This can be attributed to the collective effect of demographic explosion, high population density, a large vehicle fleet, commercial establishment, poor waste and disposal management etc.

The relationship between pollutant emissions and gaseous concentration affecting human health and ecosystems is nonlinear[6-8]. This increases the importance of the proper management for appropriate emission control strategies. The environment and human health are significantly impacted by the release of chemical compounds into the atmosphere from both anthropogenic (connected to humans) and biogenic (occurring naturally) activities. These compounds can undergo various physical and chemical reactions that have a variety of outcomes.

Photochemical process: Numerous substances in the atmosphere are involved in photochemical processes that are fueled by sunlight. For instance, interactions among nitrogen oxides (NOx) and volatile organic compounds (VOCs) brought on by

sunlight from human activities, such as vehicular emissions, can result in ground-level ozone and other pollutants, which contribute to the development of smog.

Acid Deposition: Sulfuric acid and nitric acid are produced when release of sulphur dioxide (SO_2) and nitrogen oxides (NOx) from power stations and industrial activities interact with atmospheric water vapour. These acids have a deleterious effect on ecosystems, forests, and aquatic environments when they are deposited on the Earth surface as acid rain or dry deposition.

Chemical transport: Chemical transport of released substances can take place in the atmosphere, affecting areas far from their original sources. For instance, contaminants like black carbon, ozone, and aerosols can travel across long distances, triggering poor air quality and climate change effects in far-flung regions.

Stratospheric Ozone depletion: Depletion of stratospheric ozone is caused by a number of human substances, including halons and chlorofluorocarbons (CFCs). These substances cause the release of chlorine and bromine atoms into the upper atmosphere, which can damage ozone molecules. Increased exposure to harmful ultraviolet (UV) radiation from the decreasing ozone layer could have a negative impact on ecosystems and people's health.

In order to analyse and reduce these chemicals adverse effects on the environment and people's health, it is essential to comprehend their emissions and production processes.

Secondary pollutants such as ozone (O_3) exposure are linked to aggravation of asthma, lung damage, chronic bronchitis etc. O_3 is formed in the atmosphere by the reaction of oxygen (O_2) and NO_2 in the presence of sunlight. Under favourable weather conditions, O_3 can build up to a detrimental level[9,10]. Temperature and other meteorological factors have a significant impact on ozone generation because it is a photochemical process[11].

Regional meteorology and planetary boundary layer have strong effects on the air quality of megacities like Delhi, India[12,13]. In particular, heat waves characterized by hot temperatures and sluggish weather situations are associated with the elevated ozoneconcentration[14]. Temperature influences ozone production mainly by increasing the chemical reaction rates and increasing VOCs emissions originating from biogenic processes[15]. Anthropogenic VOCs emissions do not generally increase with increasing temperature except for some evaporative anthropogenic VOCs[16]. While the formation of daytimeO_3 is characterised by photochemical reactions, a rise in nighttime O_3 is primarily due to the regional and local wind circulation mechanisms[17]. Guttikunda discussed the significance of the transportation sector in photochemical pollution (mainly NO_2 and O_3)[18]. Photochemical pollution due to ozone has become one of the most serious urban pollution menaces in Delhi, India, as it causes detrimental effects on people's health, vegetation, and materials. In addition, studies available in the literature support long-range transport of O_3via heavily contaminated locations into their surroundings[19,20].

The high level of NO_2 and CO not only results in severe consequences on the local air quality but also increases the formation of O_3. The oxidization of CO occurs in the presence of NO_2 increases the O_3 generation even in a clean atmosphere[21]. A high level of NO_2 increases the production of O_3 in a polluted environment such as traffic cross-sections by the photochemical oxidation of the unburned hydrocarbons from automobile exhaust gases[22]. Vehicular traffic and power plants are the most dominant emissions sources of NOx and CO in Delhi, NCR[1].

The measurement of air pollutant concentration is not feasible at every point in the region due to the experimental difficulties involved and the high cost of the instruments. Thus, an indirect approach such as mathematical modelling is being used increasingly for air quality analysis. Air quality models (AQMs) are commonly used to compute the pollutant concentration in the study area. AQMs are based on analytical and numerical approaches and require meteorological, topographical and emission data of the region to predict the concentration of air pollutants. The emission rate of various species plays a vital role in air quality prediction along with meteorology and topography of the data. The challenge today is to design a comprehensive emission inventory incorporating local sources. Ambient air quality monitoring is essential to evaluate the current air quality, assess the effectiveness of management techniques, and recognize and prioritise locations in dire need of preservation.

Chemistry transport models (CTMs) have the capability to deal with the gas phase chemistry, especially photochemistry. CTMs are employed in a variety of contexts, from environmental impact assessments to forecasting. It depends on how closely the CTMs and meteorological model are coupled. This can be dividedinto two categories: offline and online coupled models. In offline, a meteorological model is used first to compute the meteorological fields; then these fields are used in a CTM to obtain concentrations of various chemical species. On the other hand, online-coupled air quality models, meteorological models and CTM simulations are carried out simultaneously, trade in simulated meteorology and chemical parameters at each time step such as the Weather Research Forecast model with Chemistry (WRF/Chem)[23,24]. In the present study, an offline-coupled model WRF-Polyphemus/Polair3D is used to simulate the concentration of different air pollutants.

Emissions are a vital input parameter in air quality modeling and further, lead to many research works related to emission inventory improvement to their relevancy. An increase in the emission of different criteria pollutants increases the importance of the air quality model especially in developing countries like India. The emissions of various species show an increasing trend in Delhi, NCR[25,26]. In such a scenario, the variations of

photochemical pollutants to their emitted precursors are very important. There is also a scarcity of data not just for emissions but also for monitoring of different criteria pollutant levels. Therefore, simulated data can be useful especially wherever monitored values are not available in the study domain.

In view of the above, an attempt has been made to develop a better knowledge of thevarious responses of the gridded emission inventory over Delhi, NCR India to different forcing factors using an off-line CTM WRF-Polyphemus/Polair3D air quality modelling system.

The goal of this article is to present the simulation of gaseous species such as O_3, NO_2 and CO and their sensitivity towards the regional emission inventory of the Delhi region using an offline coupled WRF-Polyphemous modeling system.

Study Area

Delhi is located in India's northern region (Latitude 28°35′ N, Longitude 71°12′E) and is one of the highly polluted urban megacities of India.The city's eastern edge is formed by the Yamuna River, which flows through it. Delhi is located between the cooler hilly regions of the North and East, the Central torrid lands to the South and the Great Indian Desert (Thar Desert) of Rajasthan state to the West. The summers in Delhi, a semi-arid metropolis, are scorching very cold and dry winters[27]. The ambient air quality has been monitored at various sites like industrial and residential,classified by the Central Pollution Control Board (CPCB) according to land-use pattern.In this study, air quality data at three monitoring sites namely IGI (Indira Gandhi international airport site) (28.57 N, 77.12 E) and ITO (major traffic intersection site) (28.63 N, 77.24 E)and Dwarka (NSIT Engineering College) (28.75 N, 77.12 E)an institutional site (Figure-1) have been considered for the evaluation of the concentrations of simulated gaseous species.

Model description

Polyphemus-1.9.1/Polair3D: Polyphemus-1.9.1 modeling framework is used with the Eulerian CTM Polair3D (Figure-2)[28]. A CTM computes the concentration of pollutants over a given domain and a given period. It incorporates the transport (turbulent diffusion and wind advection), the chemical processes, and other fluxes like deposition, emissions, and boundary conditions.

A CTM is based on the advection-diffusion equation:

$$\frac{\partial C_i}{\partial t} + u\frac{\partial C_i}{\partial x} + v\frac{\partial C_i}{\partial y} + w\frac{\partial C_i}{\partial z} = \frac{\partial}{\partial x}\left(K_x\frac{\partial C_i}{\partial x}\right) + \frac{\partial}{\partial y}\left(K_y\frac{\partial C_i}{\partial y}\right) + \frac{\partial}{\partial z}\left(K_z\frac{\partial C_i}{\partial z}\right) + \chi_i(\vec{C},t) + E_i - D_i \qquad (1)$$

Where $\vec{C}$ is the vector of concentrations of pollutants and C_i is its ith component; u,v,w are the components of wind velocity; K_x, K_y and K_z are the eddy diffusivities along x, y and z directions respectively; $\chi_i(\vec{C},t)$ stands for the chemistry (production and loss as a result of chemical processes); E_i is the emission rate of i^{th} pollutant; D_i is the deposition flux.

Polair3D is a Eulerian3D CTM developed at ENPC (Ecole Nationale des Ponts et Chaussees) and developed to manage a broadarea of applications from modelling aerosols to photochemistry and passive transport[29]. Polair3D has been used for many applications such as ozone and NOx at the global level or a regional scale[30,31].

Polair3D is part of the Polyphemus modelling system, which includes databases, libraries of physical parameterizations (such as the Atmo Data library), and programs. It is accessible under the GNU General Public License at http://www.enpc.fr/cerea/polyphemus[30]. Programs make up Polair3D's pre- and post-processing. Using the AtmoPy library, post-processing entails displaying and computing model-to-data metrics in accordance with US Environmental Protection Agency (EPA) guidelines.

Database and Parameterization: The pre-processing stage generates input data files from the database for which we must choose between different physical parameterizations, such as those proposed by Louis and Troen and Mahrt[32,33]. To solve the partial differential equation (PDE) (1), the wind field (*u, v, w*) is obtained from the WRF model. Various meteorological factors such as temperature, skin temperature, pressure, wind field, Richardson number, boundary layer height, vertical diffusion coefficients, liquid water content, cloud attenuation coefficients, specific humidity, solar radiation intensity etc.need to be prepared for the simulation of CTM Polair3D. Parameterized fields like eddy diffusivity are estimated from raw meteorological outputs. For regional scale simulation, horizontal diffusion coefficients K_x and K_y are set to 500 m^2s^{-1}.

In the CTM Polair3D, Louis parameterization is used to compute the vertical diffusion coefficient in the PBL[32]. Further, Troen and Mahrt parameterizationis used to overwrite the vertical diffusion coefficient K_z within the boundary layer height computed by Louis parameterization[32,33]. Louis parameterization is valid for both the surface and outer layer (complete boundary layer). In the outer layer, eddy fluxes are computed as diffusive fluxes based on diffusion coefficient K, which is a function of height, shear and stability. Although these parameterizations are quite old, they are appropriate for coarser grids in the study domain.

Deposition: Deposition flux D_i in equation (1) is evaluated by $D_i = v_iC_i$, where v_i is the deposition velocity of the i-th species. Ground variables (land-use coverage, roughness, deposition velocities) for gases are calculated according to Wesely or Zhang[34,35]. There are two options for the land use cover: the USGS (United States Geological Survey) land cover map (24 categories) or the Global Land Cover Facility (GLCF) dataset (14 categories). In the present research, land use cover is derived from the USGS dataset and transformed into Zhang categories in order to calculate deposition velocities[35].

To estimate the roughness distribution, the land use cover calculated from the USGS dataset is used. For gaseous species, below-cloud scavenging (washout) is parameterised according to Sportisse and Dubois and dry deposition velocities are computed using Zhang[36,37].

Emission: In equation (1) E_i is the emission rate of various chemical species and reaction terms $\chi_i(\vec{C}, t)$ depends on spatial variable x and time t. To solve equation (1), the emissions of species such as NO_X, CO, SO_2, PM_S, Non-methyl volatile organic carbons ($NMVOC_S$) etc. are required. For which, two emission inventories (1) emission database for global atmospheric research (EDGAR) and (2) regional emission inventory is used for this study[25]. The photochemical module is used with polair3D to simulate gaseous species especially. Chemical reactions of Carbon Bond (CB05) chemical mechanisms are considered to generate anthropogenic surface and volume emissions[38]. Emissions from the various sectors in the regional emission inventory have been computed as follows[25].

Emissions from Vehicles

$$E_{i\,(Vehicle)} = \sum_j \left(Veh_j \times D_j\right) \times EF_{i,j,Km}$$

E_i is the emission of i^{th} pollutant; Veh_j is number of vehicles per type (j); D_j is the distance travelled by per vehicle in per year or vehicle utilization factor (j); $EF_{i,j,Km}$ is the emission factor of pollutant (i) for different type of vehicle (j) per kilometer driven.

Emissions from Power Plants: The amount of fuel consumed is estimated using Gurjar and Sindhwani[25,26,40]. The gross-electric generation by a power plant is measured in gigawatt-hours (GWH)[, 41].

Gross Generation (GWH) = PLF (%) × capacity × 24 × 365
Fuel use in kilo ton (kt) = Gross Generation × fossil fuel use per GWH
where plant load factor (PLF) of the different power plant is taken from the report issued by Central Electricity Authority (CEA).

Emissions from Industries, Construction Activities and Brick-Kilns

$$E_{i\,(Industries)} = \sum\left(Fuel_j \times EF_{ij}\right)$$

where, E_i is the emission per tons of pollutants(i); $Fuel_j$ is consumption of fuel per fuel type (j) (Kt); EF_{ij} is emissions of pollutants (i) per unit of energy (j) (g/kg)[41].

Emissions from Diesel Generator Sets in Residential and commercial Sector
Emissions from generator sets (gensets) are computed using the following equation[43].

$$E_{i\,(Genset)} = \sum_j \left(P_j \times E_{ij}\right)$$

Where E_i is the emission of i^{th} pollutant; P_j is the power rating of the genset (Kw) and E_{ij} is the Emission factor (g/Kwh).

Emissions from the residential sector especially due to fuel consumption in the domestic sector are computed by using the same equation adopted for emissions from industries, construction activities and brick-kilns.

Air pollutant emissions as a result of open solid waste burning have been calculated using the following formula[3,].

$$P_j = \sum_j \left(650 \times 0.1 \times p \times EF_j/86400\right)$$

where, P_j is the emission of pollutant j (g/s); p is the human population; EF_j is the emission factor of pollutant j (g/kg).

The emission from aircrafts is calculated from (International civil aviation organization (ICAO) emission data bank)

$$E_{i\,(LTO)}(inkg) = \sum_{AllAircrafts} (\text{Number of LTO cycles of aircraftj}) \times (\text{EF}_\text{i})$$

Fuel Consumption (in kg) =

$$\sum_{\text{All Aircrafts}} (\text{Number of LTO cycles of aircraft j}) \times (\text{Fuel Consumption})$$

where Landing and Take-off (LTO) cycle comprises of all activities near the airport that take place below the altitude of 3000 feet (1000 m). Therefore, the emission rate E_i in equation (1) is the sum of the total emissions from various sectors considered in the study domain. The emission rate E_i of i^{th} pollutant can be expressed as:

$$E_i = \text{E}_\text{i (Vehicles)} + \text{E}_\text{i (Industries)} + \text{E}_\text{i (Power Plants)} + \text{E}_\text{i (Waste Disposal)} + \text{E}_\text{i (Gensets)} + \text{E}_\text{i (Aircrafts LTO)}$$

Initial and Boundary Conditions

Stiff differential equations that describe the time evolution of chemical species in the atmosphere are found in equation (1) in three dimensions. These equations require initial conditions (IC) and boundary conditions (BC) to be solved. At the start of the simulation, ICs are defined inside the simulation domain, whereas BCs are prescribed during the simulation. BCs (flux conditions) are provided at both the top and bottom of the domain. At the ground, as the vertical wind velocity is null, dry deposition is applied as BCs for diffusion

$$-\rho K \nabla \frac{C_i}{\rho}.n = E_i - v_i^{dep} C_i$$

where n is upward unit vector, E_i is surface emissions and v_i^{dep} is dry deposition velocity provided as a parameterization based

on meteorological data and land use cover[28]. Initial and boundary conditions for the current investigation were interpolated using simulations of the Model for Ozone and Related Chemical Tracers, version 4 (MOZART-4) on a coarser grid for the year 2010. MOZART-4 is an offline global CTM especially suited for the tropospheric studies[44]. MOZART-4 mechanism includes 157 thermal gas-phase and 39 photolysis reactions, 85 gas-phase species along with 12 bulk aerosol compounds.

Polair3D solve the reactive-transport equation using operator splitting as advection is integrated at first then diffusion and lastly the chemistry. The direct space-time-third order scheme with a Sweby-type flux limiter is used for advection[45]. Second-order Rosenbrock method is utilized to solve the diffusion and chemistry process[46].

The ATMODATA library is used to execute physical parameterizations and pre-processing of input fields, such as ground fields, meteorological fields, emissions, initial and boundary conditions.

Further, simulated value has been analyzed and visualized over the study domain.To compare models and data, post-processing utilities are available, particularly the Python package ATMOPY. The pictorial representation of various working stages of the Polyphemus modeling system is shown in Figure-2.

WRF Simulations: Meteorological parameters are calculated by processing of WRF output data. The WRF version 3.6, which evolved through the joint efforts of multiple research institutions under the direction of NOAA, NCAR, and DOE/PNNL, is used in this study (http://ruc.noaa.gov/wrf/WG11/). The simulation domain is defined on a Mercator projection centered at 28.7°N, 77.1°E. The model setup for surface phenomena combines the NOAH Land Surface model, the Rapid Radiative Transfer Model (RRTM), long-wave radiation scheme and the Lin microphysics scheme[47-49]. The Yonsei University (YSU) boundary layer technique is used to parameterize the vertical sub grid scale fluxes resulting from eddy transportation in the ambient troposphere and the planetary boundary layer (PBL)[50]. In order to calculate atmospheric shortwave radiation, the Goddard scheme is utilized because it is more suitable with the gas-phase chemical process and the photolysis scheme, specifically the Carbon Bond mechanism (CB05), the Regional Acid Deposition Model, Version 2 (RADM2) technique, and the Regional Atmospheric Chemistry Mechanism (RACM) (Table 1)[39,51-53]. The Fast-J photolysis scheme has been used to calculate the photolysis frequencies[54]. Topography and land use were interpolated at a spatial resolution of 30" using USGS 24 classification category land-use data. The initial and boundary meteorological conditions required by the model are provided by six-hourly NCEP Final operational Global analysis data (FNL) with a resolution of 1°x1°. The majority of fields are transformed from the WRF grid to a conventional grid, which displays elevations in meters in the vertical and latitude/ longitude in the horizontal direction. The initial step in the WRF-meteo program is to calculate the elevation of the WRF strata and transform the latitude/longitude Polyphemus grid coordinates to Lambert, Mercator, or stereographic WRF grid coordinates for interpolations. For effectiveness, horizontal interpolations are carried out in the WRF grid. WRF fields are used to calculate the pressure.

Table-1: Different parameterization approaches were chosen for the WRF investigation.

Physics and Chemistry Options	Configuration Used
Microphysics	Lin et al. scheme[49]
Long Wave Radiation	RRTM Long wave
Short Wave Radiation	Goddard Short Wave
Surface Layer	Monin Obukhov Scheme[55]
Land Surface Model	NOAH LSM
Boundary Layer	YSU Scheme
Photolysis Option	Fast J Photolysis
Cumulus Parametrization	Kain–Fritsch[56]

Chemical Mechanism (CB05): Unlike CB–IV, which contains 36 species and 93 reactions, the core CB05 mechanism includes 51 species and 156 reactions. A longer set of inorganic reactions (such as those involving H2 and NO3), updated kinetic data for the rate constant expressions, updated photolysis rate data, and improved depiction of the atmospheric chemistry of ethane, greater aldehydes, alkenes with internal double bonds (inner olefins) (such as 2-butenes), oxygenated products and intermediates (such as higher organic peroxides and peroxycarboxylic acids), and terpenes are all part of the CB05 mechanism. Using smog chamber data from the University of North Carolina, Chapel Hill, and the University of California, Riverside, Yarwood and team assessed the CB05 mechanism and discovered that, essentially it performed well or in some instances, even better than the previous version CB–IV in simulating the smog chamber data[39]. Ozone produces by CB05 is faster due to greater radical production from ALDX photolysis than ALD2 photolysis. Further, the conversion rate of NO to NO_2 is simulated well by CB05 than CB04[39].

Emission Computation and Distribution: Surface and volume emission for gaseous substance along with NMVOCs are computed according to the CB05 chemical mechanism. The Institut fu¨r Energie-wirtschaft und Rationelle's speciation for urban conditions and CORINAIR's speciation for continental contexts provide the relationships to actual species. The global 2010 anthropogenic emission data from the EDGAR database

have been used for the study area. It consists of annual emitted quantities, given for the different activity sectors and NO_X, CO, SO_X, NMVOCs, $PM_{2.5}$, PM_{10} and NH_3. EDGAR emission inventory having spatial resolution of 0.1°x 0.1° is used over the region comprised of the whole national capital region (NCR) Delhi, India ranging from 75.2°E to 79°E longitude and 26.8 °N to 30.6°N latitude. Further, the regional emission inventory of spatial resolution 0.02° is used over the finer domain (76.76°E to 77.46°E and 28.3°N to 29°N) to incorporate the local emission sources to improve the prediction of different gaseous species[25].In the current study, regional emission inventory for pollutants is estimated for the base year 2010 for CO, PM_{10}, NO_2 and SO_2 emitted from various sources in Delhi and its fringing areas Gurgaon, Faridabad, Ghaziabad, Bahadurgarh, Noida, Greater Noida, Sonipat at a spatial resolution of 2km x 2km between 76.76°E to 77.46°E longitude and 28.3°N to 29.0°N latitude. Regional emission inventory incorporates emissions from Industrial sources, power plants, brick kilns, household sources, on-road vehicular sources, waste, road dust and landing and take-off cycle of aircraft emissions. Model configuration is summarized in Table-2.

Figure-1: Inner domain for which local emission inventory is used for the study. Where ( ) are air quality monitoring sites.

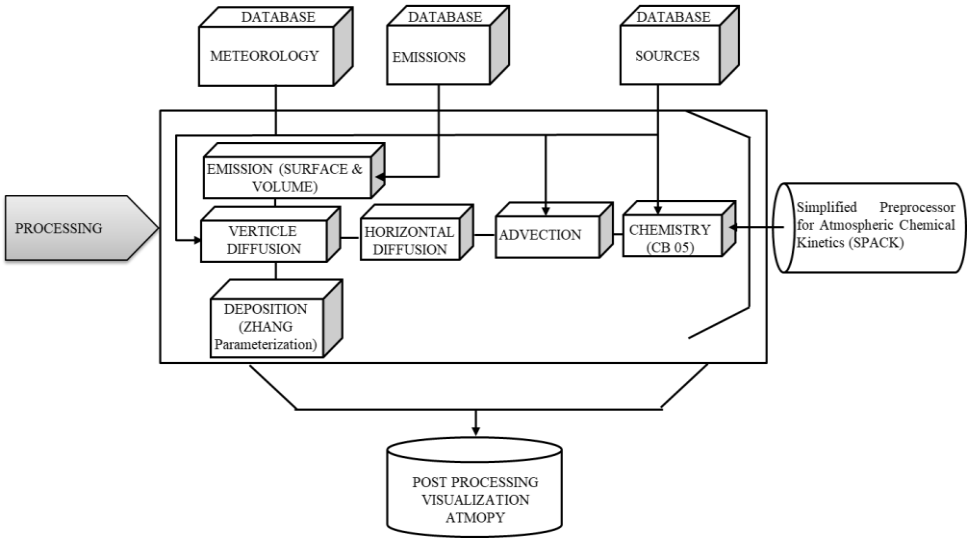

Figure-2: Flowchart of Polyphemus different working stages. It comprises of databases, libraries for data processing and physical parameterization, programs to prepare input data, and C.T.M as a driver and numerical solver. The driver is in charge of the time loop and input-output tasks to make the calls for the time integration.

Table-2: Model configurations for the study domain.

Simulation Options	Configurations of the study domain
Simulation Periods	2010.06.19 - 2010.06.24 and 2010.12.19 - 2010.12.24
Meteorological fields	WRF Ouput
Land use coverage	Zhang Categories[36]
Vertical diffusion coefficient	Inside PBL: the Troen–Mahrt's parameterization Above PBL: the Louis's parameterization[33, 34]
Horizontal Grid	10 / 2 Km
Initial and Boundary condition	Model for Ozone and Related chemical tracers Mozart – 4[44]
Dry deposition velocities	Zhang parameterization[38]
Gas-phase chemistry	CB05[39]
Emission Inventory	EDGAR and Regional Emission Inventory[25, 57]

Table-3: EDGAR and regional emission inventories used an amended allocation of gases depending on source type and varying height levels[58,59].

Source Category	Emission height of gases			
	Ground	~150m	~250m	Higher
Combustion in energy and transformation industries			8%	92%
Non-industrial combustion plants	50%	50%		
Combustion in manufacturing industry	50%	50%		
Production processes	90%	10%		
Extraction and distribution of fossil fuels	90%	10%		
Solvents and other product use	100%			
Road transport	100%			
Other mobile sources and machinery	100%			
Waste treatment and disposal	80%	20%		
Agriculture	100%			
Nature	100%			

Effective emission height significantly affects the simulated concentration values. Therefore, the vertical distribution of gaseous species applied for regional and EDGAR emission inventory according to the various source categories is given in Table-3[58,59].

Experimental Set-up: Further, the sensitivity of O_3 simulated concentration towards the emission of various species and major precursors NO_X; VOCs have been assessed using different simulation scenarios. These simulations are: i. Base case simulation. ii. Two simulations in which all species emission is abated by 50% and 100% respectively. iii. Two simulations (a) NO_X emission abated by 20% (b) VOCs emission abated by 20%, iv. Two simulations (a) NO_X emission abated by 50% (b) VOCs emission abated by 50%, v. Two simulations in which both NO_X and VOCs emissions reduced contemporarily by 20% and 50% respectively.

Further, the impact of emission reduction on O_3 simulated concentrations has been analyzed using Thunis and Clappier methodology[60]. A change in relative concentration driven by a change in relative emission is termed as relative potency defined for different simulation scenarios as above.

$$P_\alpha^k = \frac{\Delta C_\alpha^k}{\alpha C} \; ; \; P_\alpha^{All} = \frac{\Delta C_\alpha^{All}}{\alpha C}$$

where k is the selected major precursors NO_X and VOCs, α is the reduction level of emission (20% or 50%) and "All" represents the scenario reducing both contemporarily. C denotes the concentration of O_3 from base case scenario and $\Delta C_\alpha^k = C_\alpha^k - C$ is the change in concentration between the various simulations and base case simulation scenario. The maximum change in the concentration of O_3 due to the change in the precursors reaction might be the result of the reduction of a particular or because of a simultaneous decrease in all the precursors considered termed as maximum potency (I_{max}). The maximum potency (I_{max}) generally equal to P_α^{All} can also occur due to the impact of abating one precursor alone. This indicates the importance of that major precursor. If $I_{max} = 0$, indicates that reduction in emission have no effect on the concentration level of O_3, be close to -1 when emission reductions are completely effective, they lower concentration levels in the same proportion, but they can also have a positive consequence when they raise concentrations overall.

Results and Discussion

To understand the air quality of a megacity, consideration must be given to the different emission sources in the region. The concentration of various gaseous pollutants proportionally depends on the emission sources. The comprehension of the quantitative relationship between ambient pollution levels and atmospheric emissions is important to control the emission sources. To understand this relation for primary pollutants like SO_2 and CO is straightforward, as the ambient pollution levels are proportional to emissions because the pollutants of interest are the pollutants that are emitted in the atmosphere. However, the air quality regulation for the secondary contaminants, such as O_3 depends on various additional parameters to address. Ozone generation only occurs to a considerable degree in the troposphere., which occurs due to photolysis of NO_2 at wavelengths less than 424 nm, when sufficient solar energy absorbed by NO_2 causes photo dissociation[61].

$NO_2 + h\nu = NO + O\ (^3P)$
$O\ (^3P) + O_2 + M = O_3 + M$
$NO + O_3 = NO_2 + O_2$
i.e. O_3 level is related mainly with the NO_2/NO concentration ratio during daytime.

In the polluted urban areas, the VOC and NOx chemical processes used to predominate. Over methane and its byproducts of degeneration[62-65]. An O_3 precursor like CO is ubiquitous in the atmosphere, which has various natural and anthropogenic sources. Biomass burning, VOCs, combustion processes are the main sources of CO, which have a longer lifespan of the order of a few months. As O_3 is a secondary pollutant depending on the photochemical reaction and its major precursors, e.g. NO_X, CO, VOCs. A regional emission inventory is able to capture the local emission sources in Delhi for primary pollutants NO_2, NO, CO and SO_2 whereas, EDGAR is not able to capture the emission sources due to the lack of the incorporation of various regional sources, contributing to the emission level of hazardous gaseous pollutants in the megacity Delhi.

Significant under-prediction of NO, NO_2, CO and SO_2 from the CTM model Polair3D using global inventory makes it necessary to look towards the regional emission inventory to enhance the performance of the CTM. Further various statistical metrics is used to assess the performance of CTM Polair3D using EDGAR and regional emission inventory for the prediction of gaseous pollutants.

Assessment of Emission Inventory: Spatial plots of mean surface emission values from EDGAR and regional emission inventory have been compared during the simulation period of summer and winter period. Clearly regional emission inventory is able to capture local sources in a better way than the global emission inventory EDGAR (Figure-3). Figure-3 ((b), (d), (f), (h)) show that the spatial mean anthropogenic emission values of CO, NO_2, $SO_2$from global inventory are lesser (Figure-3(b) (d), (f), (h) in comparison to the corresponding mean spatial distribution obtained from regional emission inventory (left panels of Figure-3). Besides the administrative and political centre of the country, Delhi is one of the major manufacturing hubs of various sectors such as electrical and electronics, home consumable industries, textiles, leather, metals, machinery, pharmaceuticals etc. Service sectors (hotels, tourism, IT, banking etc., in Delhi, NCR are also contributing towards the emission of various pollutants. Power sectors like NTPC, North Delhi power limited, Delhi power Supply Company limited, Pragati power plant etc., located in the study region act as the main contributing sources of CO, SO_2, NO_X etc.

The aviation sector is also developing stupendously in Delhi, NCR. The fuels used in the aircrafts have high emissions of NO_X. Landing, take off and cruises are further contributing to the emission of black carbon, dust, methane etc. Apart from vehicular emission sources construction and real estate sectors are also one of the major contributing stakeholders towards the emission of different air pollutants. This is clearly evident from the mean emission plots in Figure-3 (b),(d),(f),(h). The global EDGAR-HTAP emission inventory is not showing any sensitivity to the emissions of various gaseous species in the study region despite the presence of many contributing sectors. Therefore, an attempt has been made to include diverse anthropogenic sources of air pollution in the study area by considering a regional emission inventory in the present study.

Model performance for gaseous species: The simulated mean spatial concentrations of CO, NO_2, SO_2 and O_3 by using global and regional emission inventory are compared at the ground level for summer and winter simulation period of the year 2010. The simulated mean concentration of O_3 during the summer period (Figure-4(a),(b)) is higher in comparison to winter simulation period of the year 2010 (Figure-5(a),(b)). The mean spatial concentration of NO_2, simulated by using EDGAR is severely low (Figure-4(d),5(d)) in comparison to the corresponding mean spatial plot of NO_2 simulated with regional emission inventory (Figure-4(c),5(c)) during summer and winter simulation period as well. Similar results can be seen in the case of CO also (Figure-4(f), 5(f) and 4(e), 5(e)).

In the case of NO_2 global emission inventory is not able to capture the concentration distribution and further shows good agreement with the emission distribution of NO_2 with EDGAR-HTAP (Figure-3 (e)). Further, the mean spatial simulated concentration plot of NO_2 from the regional emission inventory (Figure-4(c), 5(c)) is able to capture the hotspot in the study domain as it can be seen from the spatial mean plot of NO_2 emission (Figure-3(b)) from the same inventory.

The mean spatial concentration plot of NO_2 during summer simulation period Figure-4(c) is lesser than the corresponding plot in winter period Figure-5(c). This can be attributed to the longer lifetime of NO_2 during wintertime, which allows a longer-range transport. The mean spatial concentration of CO is also showing good agreement with the mean spatial distribution of CO emission (Figure-3(a), 4(c), 5(c)).Similarly, the mean spatial concentration of SO_2 over the study region (Figure-4(g), 5(g)) is showing good agreement with the emission distribution of SO_2 (Figure-3(c)).

Secondary pollutant O_3 mean spatial distribution depicted in Figure-4(b) and 5(b) represent the concentration of O_3 for summer and winter simulation period using global inventory over the study area. Similarly, Figure-4(a) and 5(a) represent the mean spatial distribution of O_3 using local emission inventory for summer and winter season respectively.

Mean spatial distribution of O_3 over study region is higher in summer simulation period than winter. This can be attributed to the higher temperature in summer season helpful for photochemical reaction in the presence of sunlight. Contrary to the NO_2, CO and SO_2simulation from regional inventory (Figure-4(a), 5(a)), EDGAR emission gives higher mean spatial O_3 concentration (Figure-4(b), 5(b)) over the study region. Corresponding NO_2 mean spatial plot (Figure-4(d), 5(d)) from global inventory is showing very low value over the study region. Generally, O_3 production rate increases at low NOx and for higher NOx emissions, O_3 in the urban region either remains constant or decreases as NOx emission increases[66]. NO_2 average emission depicted through regional emission inventory (Figure-3(b) is higher than EDGAR (Figure-3 (e)).

Similarly, NO average emission from regional emission inventory (Figure-3(g)) is higher in comparison to EDGAR (Figure-3(h)) over the study domain. This further advocates the higher mean concentration of simulated O_3 through EDGAR emission (Figure-4 (b), 5(b)) instead of local emission inventory (Figure-4(a), 5(a)) during the summer and winter simulation period. Diurnal variation of simulated concentration of O_3 at IGI and ITO monitoring sites (Figure-6) is compared with the observed values. At IGI and ITO, simulated concentrations using global inventory are predicted whereas the concentrations from regional inventory are under-predicting the O_3in comparison to the observed value. Especially, at IGI diurnal concentration of O_3 from local emission inventory exhibits under prediction.

At ITO, the regional emission database is showing a satisfactory comparison with the diurnal trend of observed O_3 concentration. It has been observed that the incorporation of regional emission inventory for emission preparation increases the simulated emission and concentration of NOx, CO, and SO_2 but not for O_3 concentration.

Severe under prediction for the diurnal variation of NO_2 from EDGAR emission is found at IGI and ITO (Figure-7 (a) and (b)). Simulation of NO_2 using regional emission inventory is able to remove the severe under prediction. However, this is not able to capture the hourly variation (Figure-7 (a) and (b)).

The highersimulated mean concentration of NO_2 and NO from the regional emission inventory indicates toward the severe health risk of its exposure. Higher NOx surface emission resulted in higher NO; NO_2 simulated concentration and consequently lower O_3 concentration from regional emission inventory. Whereas, lower NOx surface emission from EDGAR resulted in lesser NO; NO_2 simulated values and higher O_3 concentration. Further comparison of hourly simulated NO_2 using global and regional emission inventory with observed concentration of NO_2 at IGI is shown in Figure-8(a) and 8 (b). Similarly, the comparison of hourly simulated NO_2 using both the emission inventory with observed NO_2 at ITO is shown in Figure-9(a) and 9(b).

Further, 8 hourly observed O_3 concentrations are compared with the simulated concentrationsfrom global and regional emission inventory at IGI and ITO sites, during the summer and winter study period respectively (Figure-10).

It has been observed that simulated O_3 concentration with global inventory exhibits a good agreement in trends with observed 8-hour average O_3 at IGI airport during the winter study period with FAC2 value of 0.94, RMSE as 38.77 and correlation value of 0.76 (Table-4). Whereas, regional emission inventory shows better agreement with observed 8-hour O_3 concentration trends at ITO. The second 8-hour average O_3concentration exceeds the standard level of 100 μgm^{-3}at the IGI airport site (Figure-10).

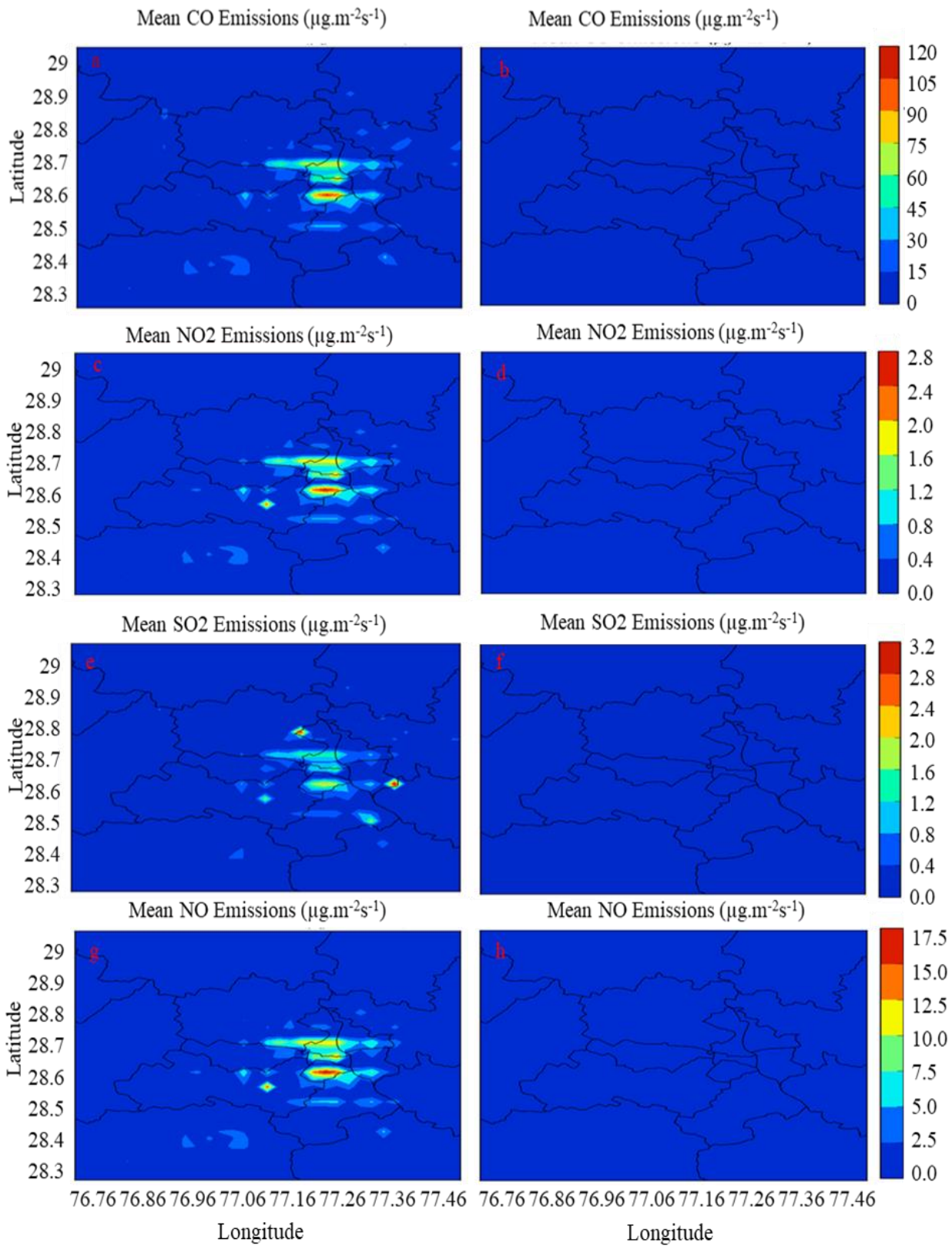

Figure-3: Average anthropogenic ground emissions (µg/m2/s) of CO, NO_2, SO_2, and NO varied spatially throughout the study area over the simulated timeframe using the regional emission inventory (left panel) and EDGAR (right panel), respectively.

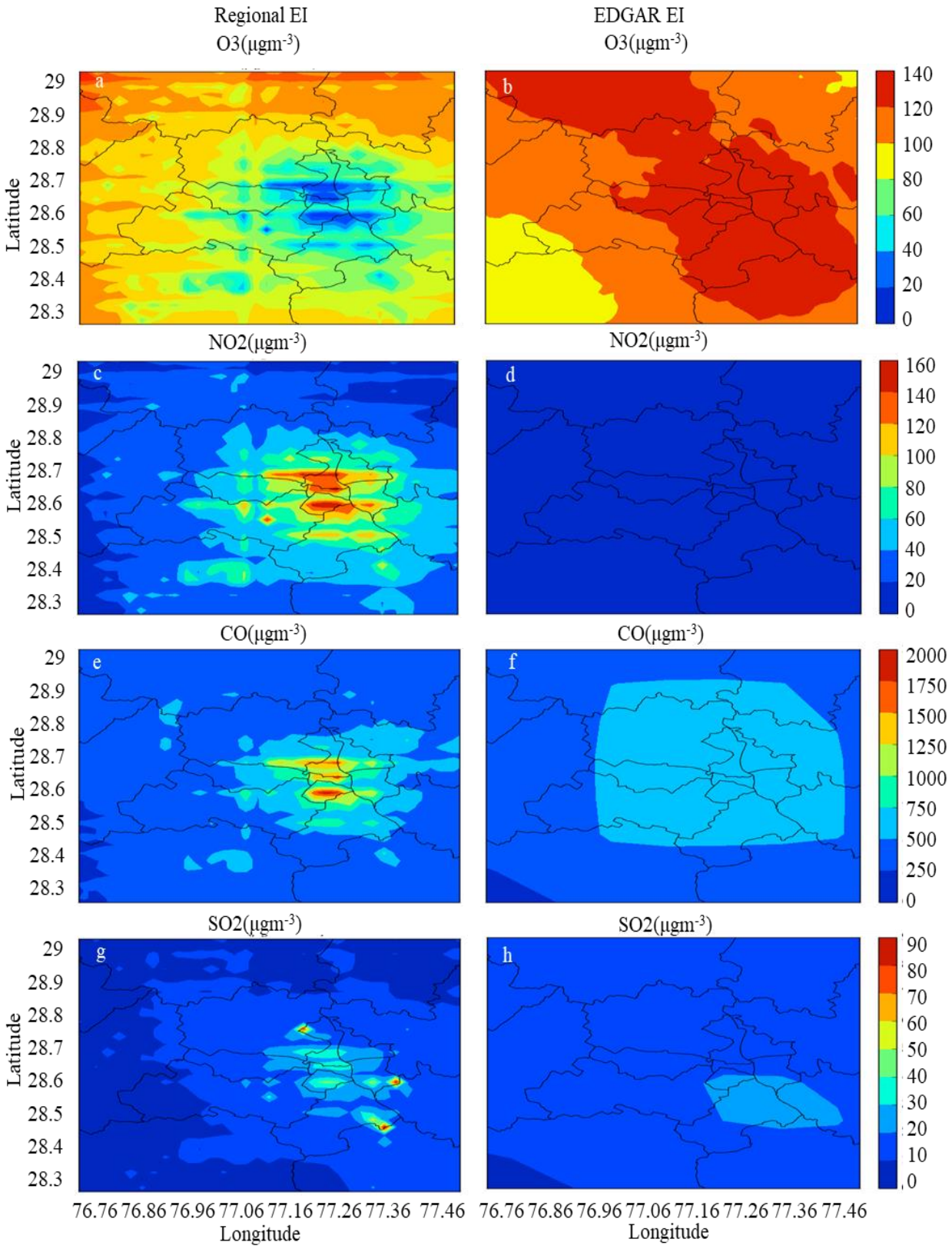

Figure-4: The average modelled concentrations of gaseous species O_3 (a), NO_2 (c), CO (e), and SO_2 (g) are plotted spatially using the regional emission inventory and EDGAR (O_3 (b), NO_2 (d), CO (f), and SO_2 (h)) for the summer simulation timeframe.

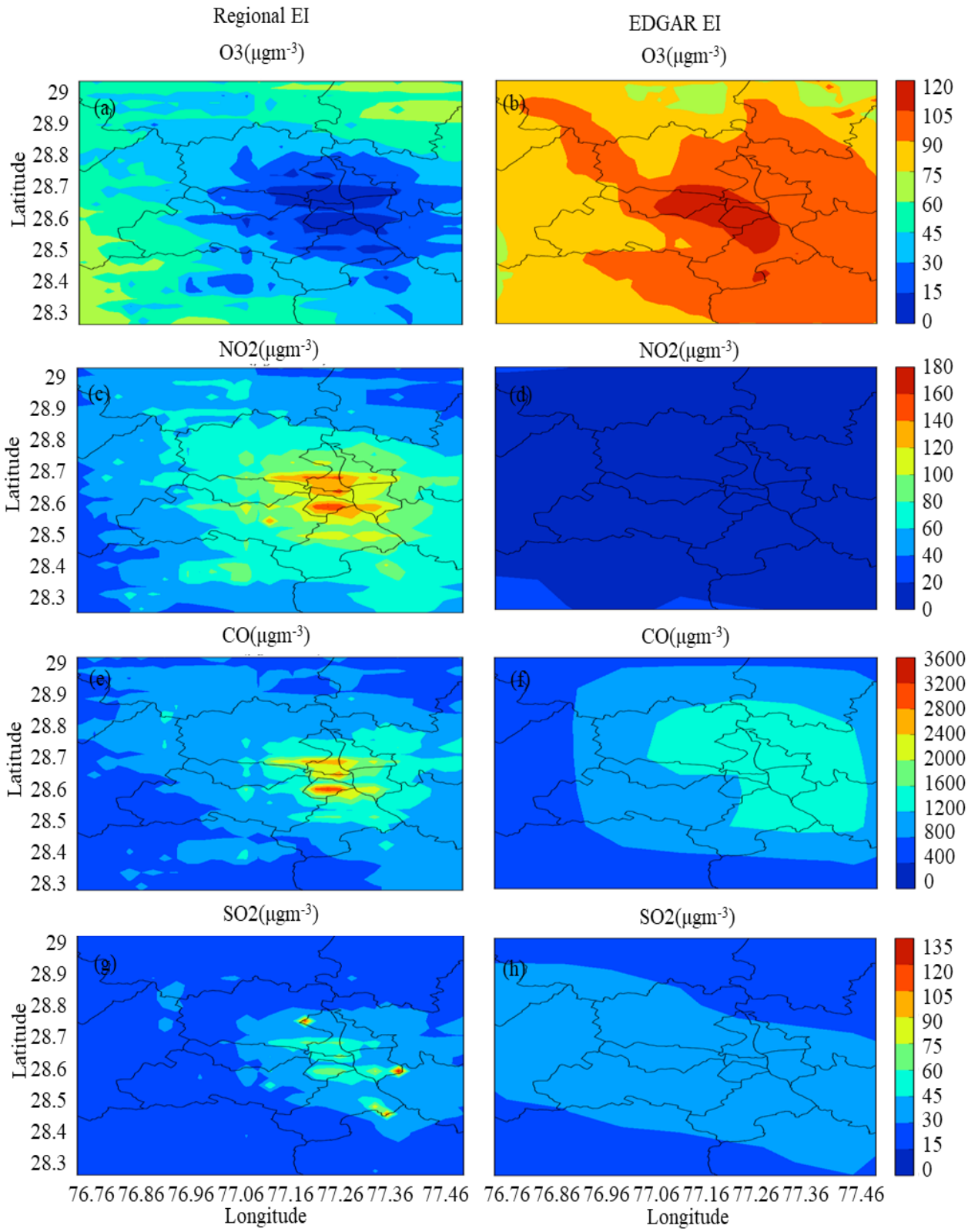

Figure-5: The average modelled concentrations of gaseous species O_3 (a), NO_2 (c), CO (e), and SO_2 (g) are plotted spatially using the regional emission inventory and EDGAR (O_3 (b), NO_2 (d), CO (f), and SO_2 (h)) for the winter simulation timeframe.

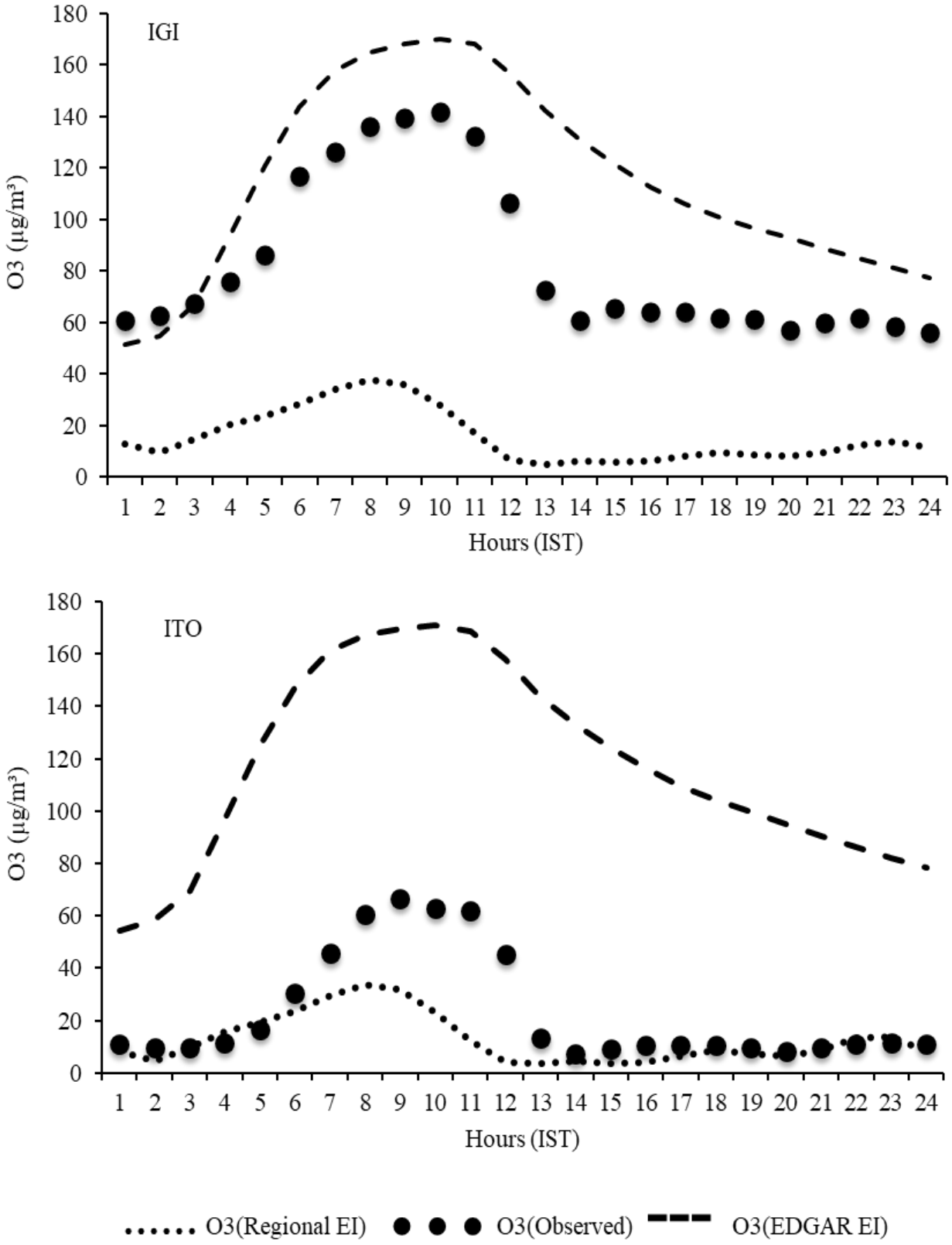

Figure-6: Using regional and EDGAR emission inventories, the diurnal variation of simulated O_3 is compared with the observed O_3 at IGI and ITO stations in the research area during the winter study period.

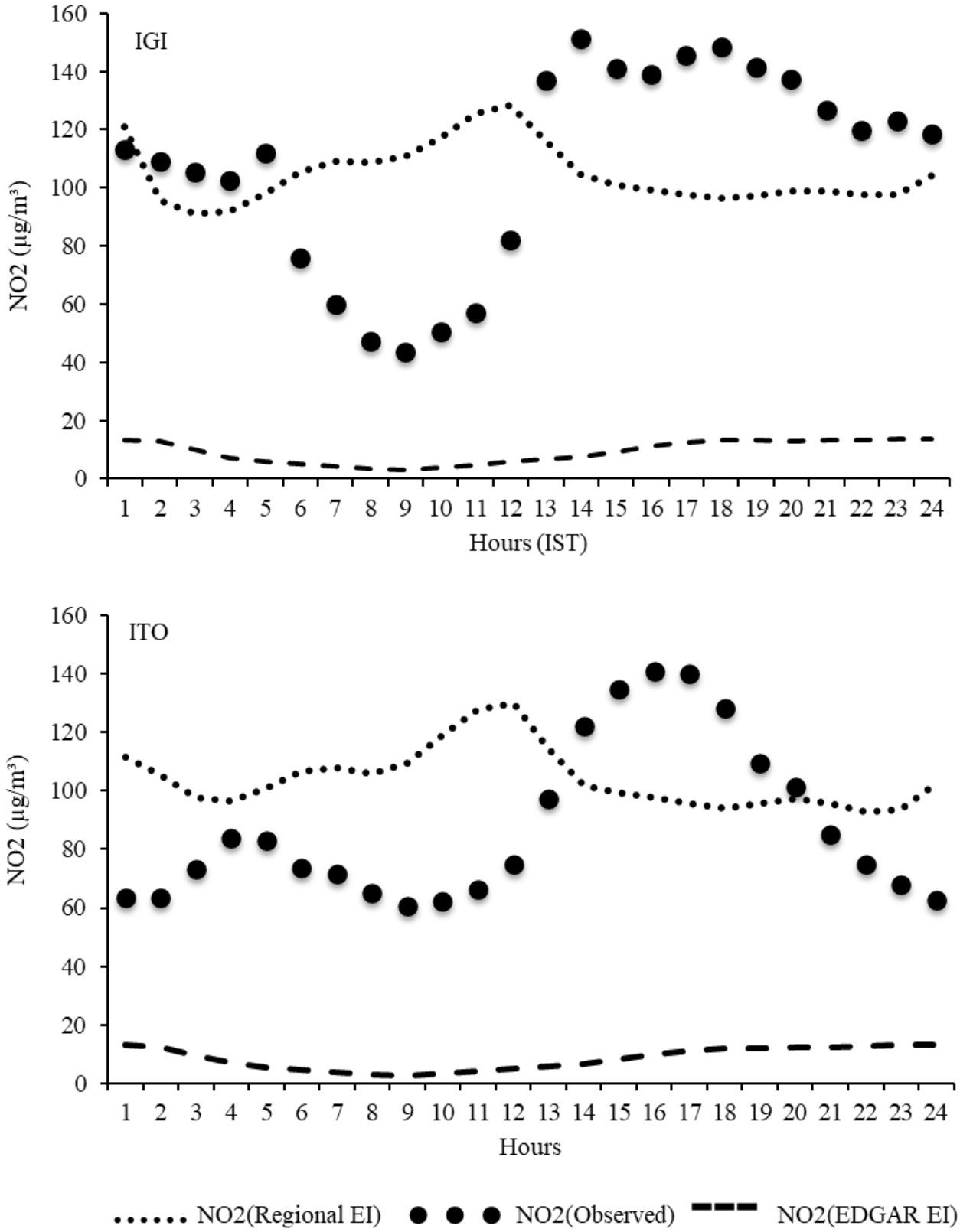

Figure-7: Comparison of Diurnal Variation of simulated NO_2 using regional and EDGAR emission inventory with monitored NO_2 at IGI and ITO sites in the study area during the winter study period.

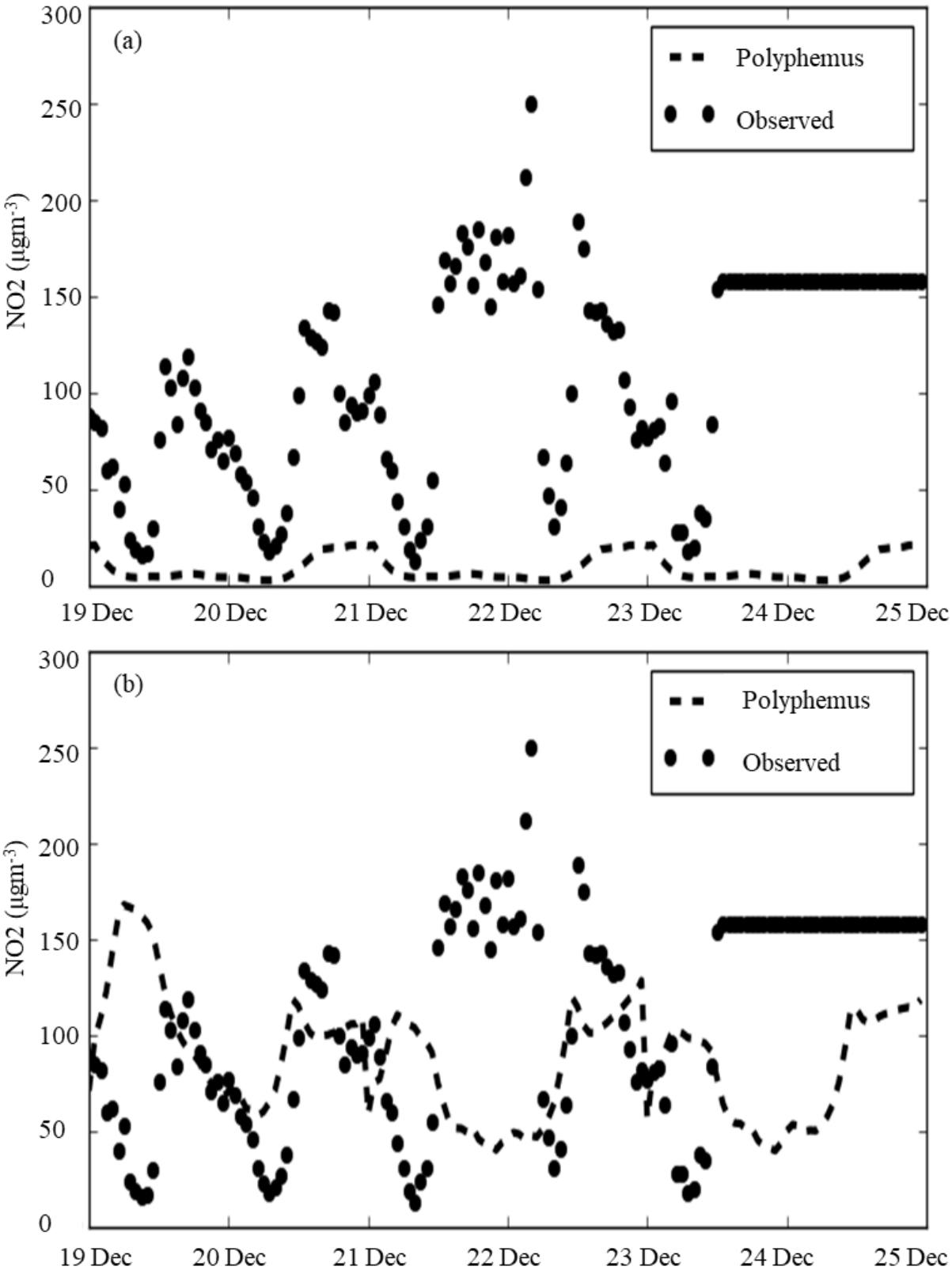

Figure-8: Comparison of temporal variation of simulated NO_2 using EDGAR (a) and regional emission inventory (b) with monitored NO_2 at IGI location in the study area during the winter study period.

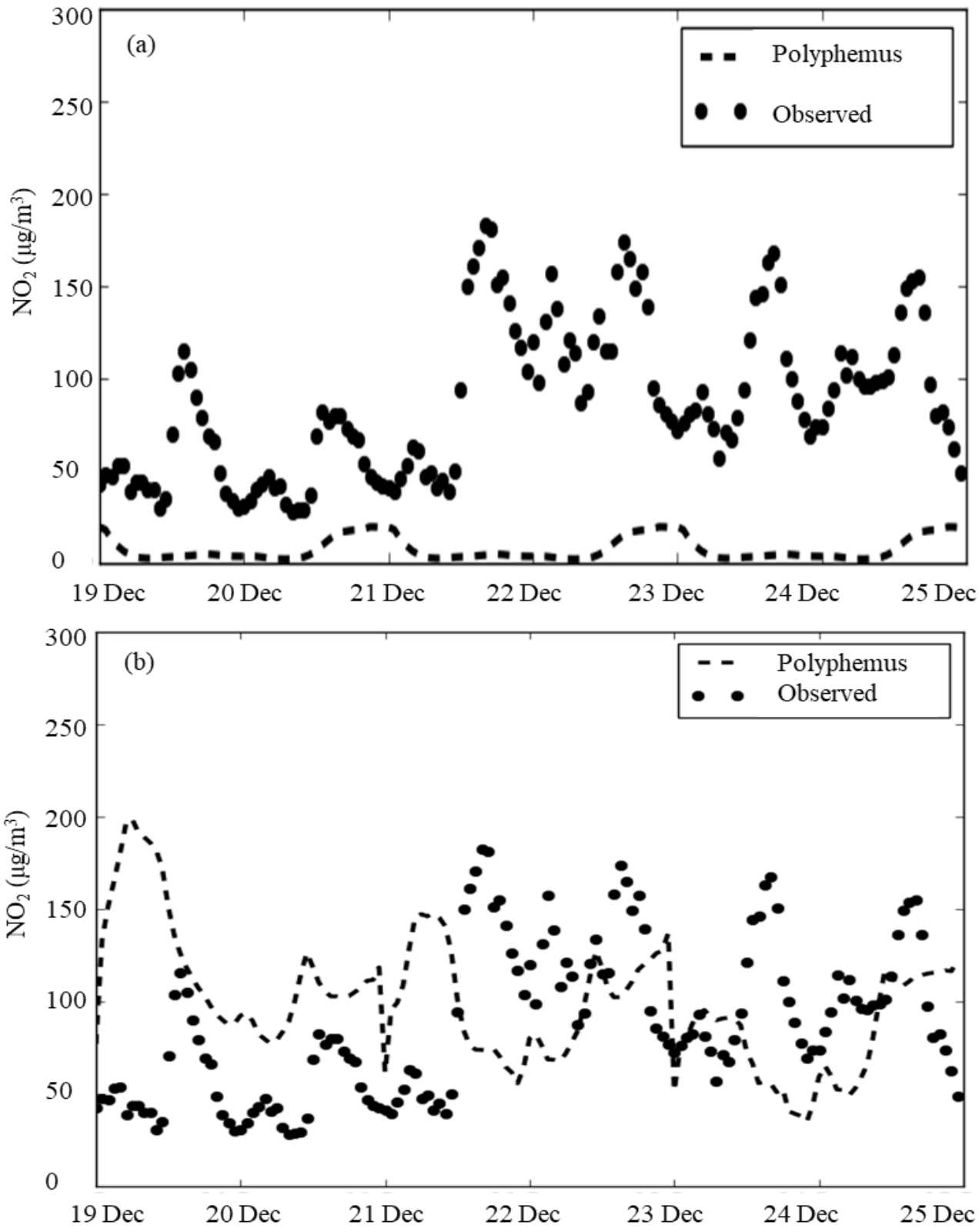

Figure-9: Comparison of temporal variation of simulated NO_2 using EDGAR (a) and regional emission inventory (b) with monitored NO_2 at ITO sites in the study area during the winter study period.

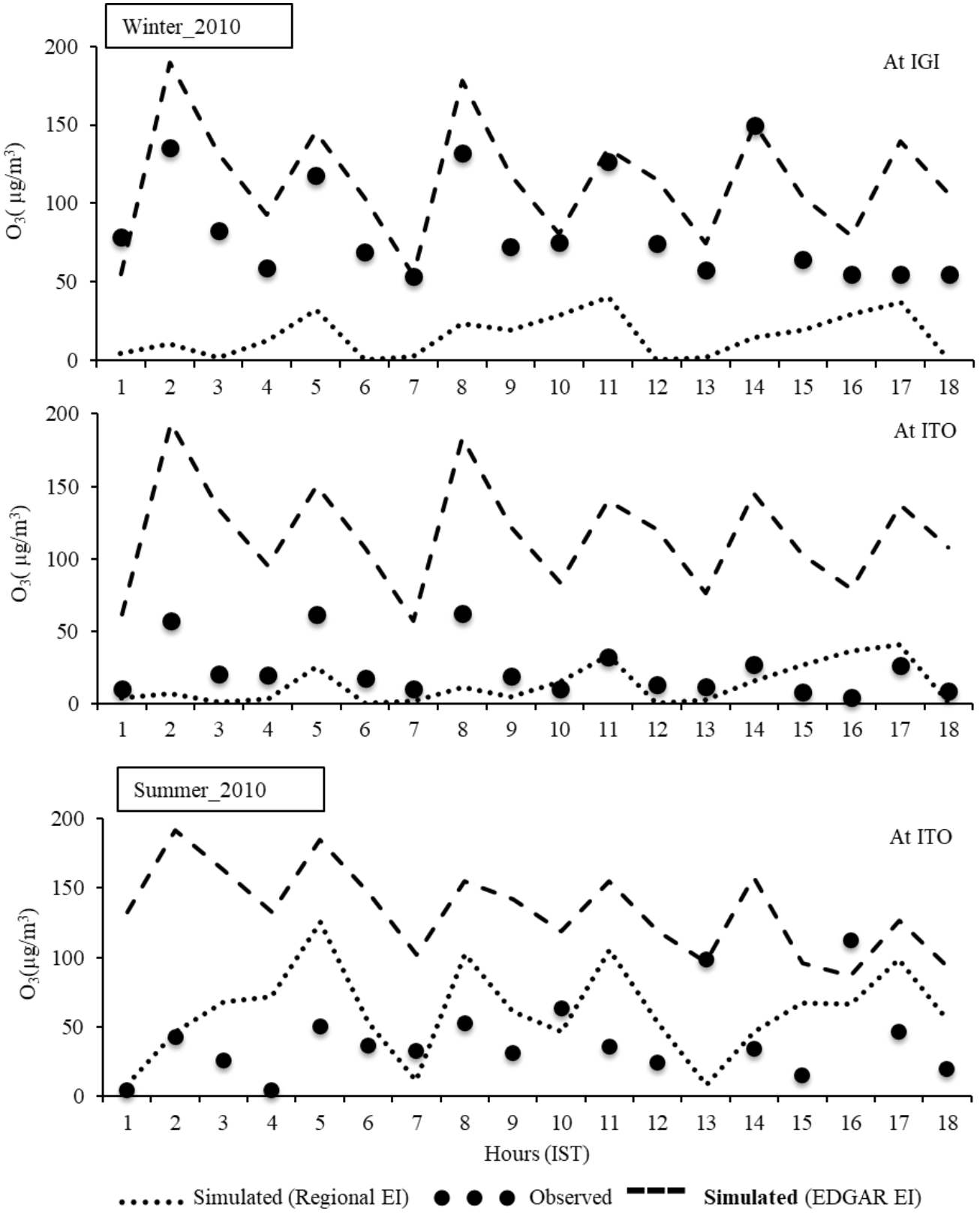

Figure-10: Comparison of observed and simulated with (regional emission inventory (EI) and EDGAR_HTAP_V2) 8 hourly average concentration of O_3 at IGI and ITO during winter and summer simulation period.

Table-4: Statistical measures to assess the model performance using regional and global emission inventory with respect to monitored and simulated 8hr average ozone value.

	Emission Inventory (EI)	FAC2	RMSE	r-Correlation
ITO-June	Regional EI	0.44	46.72	0.008
	EDGAR_HTAP_V2	0.16	103.29	-0.23
ITO-Dec	Regional EI	0.22	23.21	0.155
	EDGAR_HTAP_V2	0	96.19	0.85
IGI-Dec	Regional EI	0.11	75.03	0.28
	EDGAR_HTAP_V2	0.94	38.77	0.76

Clearly model simulations reveal that the formation of O_3 in the Delhi, NCR metropolitan region is driven not solely due to anthropogenic sources but other external factors such as transport, meteorological parameters, chemical transformation etc., also contributes immensely towards the O_3 level.

Delhi Air Quality's Dynamic Sensitivity to the Regional Emission Inventory: The study region's baseline emissions (derived from the Delhi high-resolution regional emission inventory) have been altered in accordance with the following two assumptions in order to determine the impact of the megacity Delhi on air quality: i. All of the contaminants' anthropogenic emissions decreased by 50% throughout the domain. ii. A 100% reduction in anthropogenic emissions across the domain (annihilation scenario).

As a simple method for examining the effects of megacities on the climate and air quality worldwide, the annihilation technique has been employed in megacities[67]. Mena-Carrasco and team evaluated the effects of Mexico City emissions on regional air quality and chemistry using a similar methodology[68]. To confirm whether it was wise to maintain the aforementioned strategy at a regional level or whether it would have been preferable to lower the emission variation in order to prevent significantly changing the atmospheric chemical policy in the area around the source under study, we ran two hypothetical simulations. To account for non-linear pollutants' concentration/ deposition response to emission drops off, EMEP employs the second method[69]. In contrast, de Meij and team investigated the response of contaminants to emission reduction in the Lombardia region using both 50% reduction and no emissions assumptions[70].

Response to reductions in anthropogenic emissions has been further analyzed. Comparing the outcomes of the two scenarios has revealed pertinent non-linear impacts on several species. Each surface grid point's average absolute differences between the base case and the two reduction scenarios have been compared in order to verify the dependence of concentration variation on the emission reduction rate. When the concentration variation obtained for the 100% reduction scenario for NO_2, CO, and O_3 is twice as great as the one obtained for the 50% reduction scenario, the process under study is said to be linear (Figure-11). Although O_3 exhibited substantial non-linearity, NO_2 shown more departures from linearity during the winter months (Figure-11), while CO and SO_2 exhibited linear or nearly linear behaviour. When the concentration variability brought about by emission reduction is high, such as within Delhi or the nearby areas, the non-linearity influence seems to be significant; but, when the concentration variation is low, such as far from the region where emissions have been perturbed, it is more limited. The distinct photo-chemical regime that characterizes winter season, when NOX concentrations are at least twice as high as during the summer and ozone is decreased to around one-third of its summer levels, may be the reason of the increased winter non-linearities for NO_2 and O_3. According to Finardi and team, the outcomes of the 50% emission reduction scenario have been kept for use in future scenario assessments in order to minimize the impact of non-realistic abatement rates on the chemical policy of the studied area[71]. During June and December, the scenario that reduces emissions results in the reduction of NO_2, CO and SO_2 concentration over Delhi and the surrounding region in the surface layer. This indicates that emissions from the research area result in a new generation of NO_2, CO and SO_2 during the winter and summer study period (Figure-11). During summer and winter study period the ozone produced within the surface layer of the study area experience a rise of O_3 levels is rather seen as a result of the emissions reduction scenario (Figure-11). The study domain, thus works as a local O_3 absorber during winter and summer time, when a titration effect of NO_X emissions prevails.

The megacity impact has been estimated in terms of percentage contribution to regional concentration caused by emissions from megacity Delhi (defined as 100* (NORMAL - NODEL)/ NORMAL), where NODEL stands for the 50% emission reduction scenario and NORMAL for the reference unperturbed, or base case scenario[72]. During summer simulation period NO_2 model concentration reduction lies in between 17.45% to 39.94%, CO diminishes by 5.05% to 42.38%, whereas O_3 instead exhibits an increase of 1.53% to 133.8% over all the grid points. Similarly, in winter simulation period NO_2 model concentration reduction lies in between 17.94% to 33.13%, CO

diminishes by 2.96% to 40.53%, whereas O_3again exhibits an increase of 3.57% to 104.25% over all the grid points. The maximum potency (I_{max}) is calculated for each grid cell in the study domain during the study period for the reference emission reduction levels of 20% and 50% respectively. The spatial plots for maximum potency over the study domain for the referred emission reduction level of 20% of major precursors NO_X, VOCs and NO_X-VOCs contemporarily are shown in figure 12. Three subplots in the left panels represent the variation of maximum potency during the summer study period and right three subplots for the winter study days (Figure-12). The emission reduction is found to be more effective in reducing the O_3 concentration in comparison to NO_X emission reduction and simultaneous reduction of NO_X, VOCs. NO_X emission reduction increases the simulated O_3 concentration. This can be attributed to the VOCs deficient emission inventory of the study domain. Reduction in VOCs emission reduces O_3 level, whereas abatement of NO_X emission increases O_3 level. Higher changes in O_3 concentration levels due to emission reduction have been found during summer in comparison to the winter simulation period. Due to deficient VOCs emission inventory, the referred contemporary reduction in NO_X and VOCs scenario also exhibits an increase in the O_3 level (Figure-12). This treatment will be very helpful for the policy makers in their approach of probable choice of regional abatement criteria to control and improve the air quality of the region.

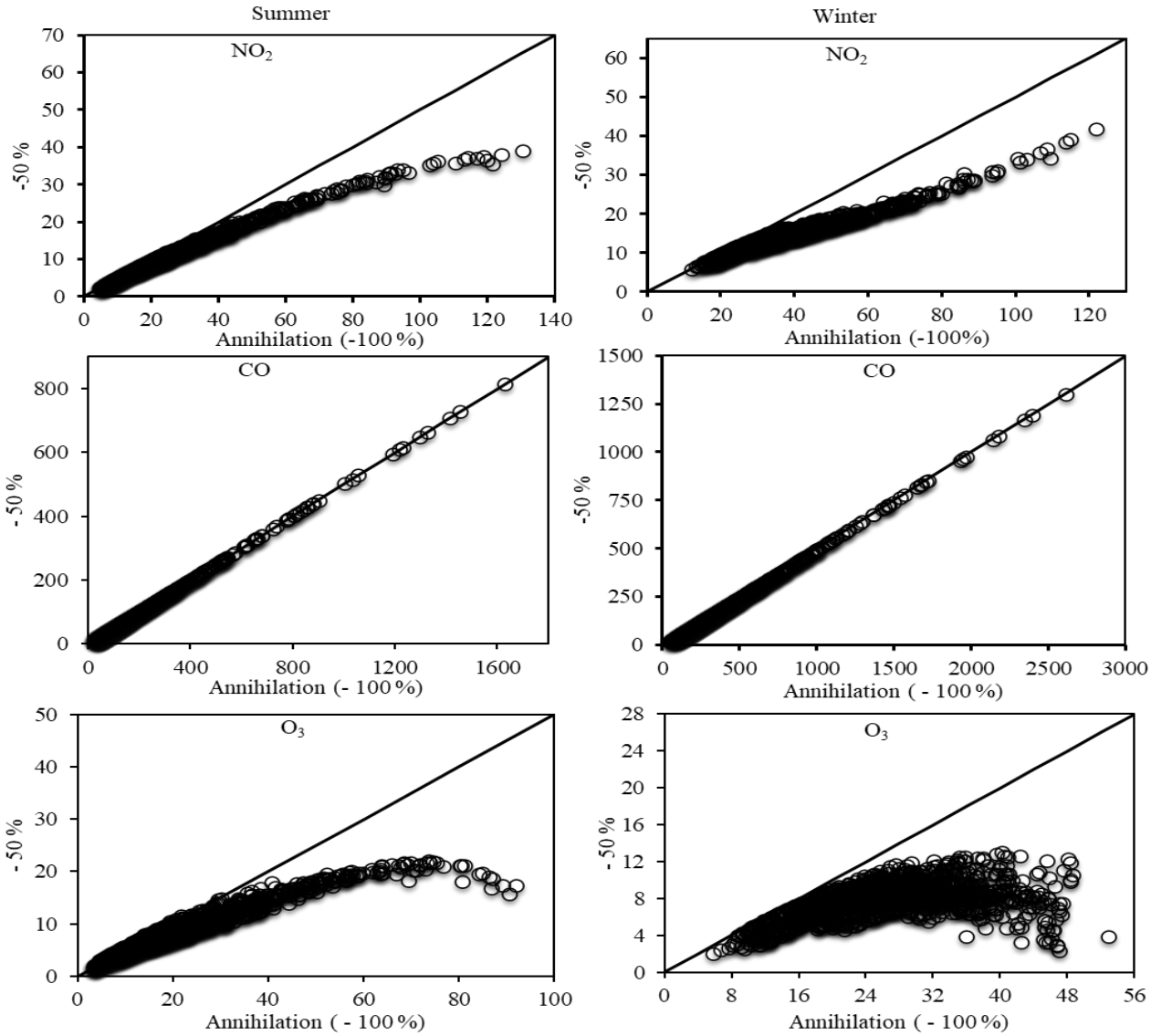

Figure-11: The base case and the 50% (ordinate) and 100% (abscissa) reduction scenarios are compared for the average absolute differences in NO_2, CO, and O_3 between June (left) and December (right) 2010; each dot represents a value at the surface grid point; the ordinate scale is half of the abscissa scale, so dots along the diagonal represent linear response to the reduction in emissions.

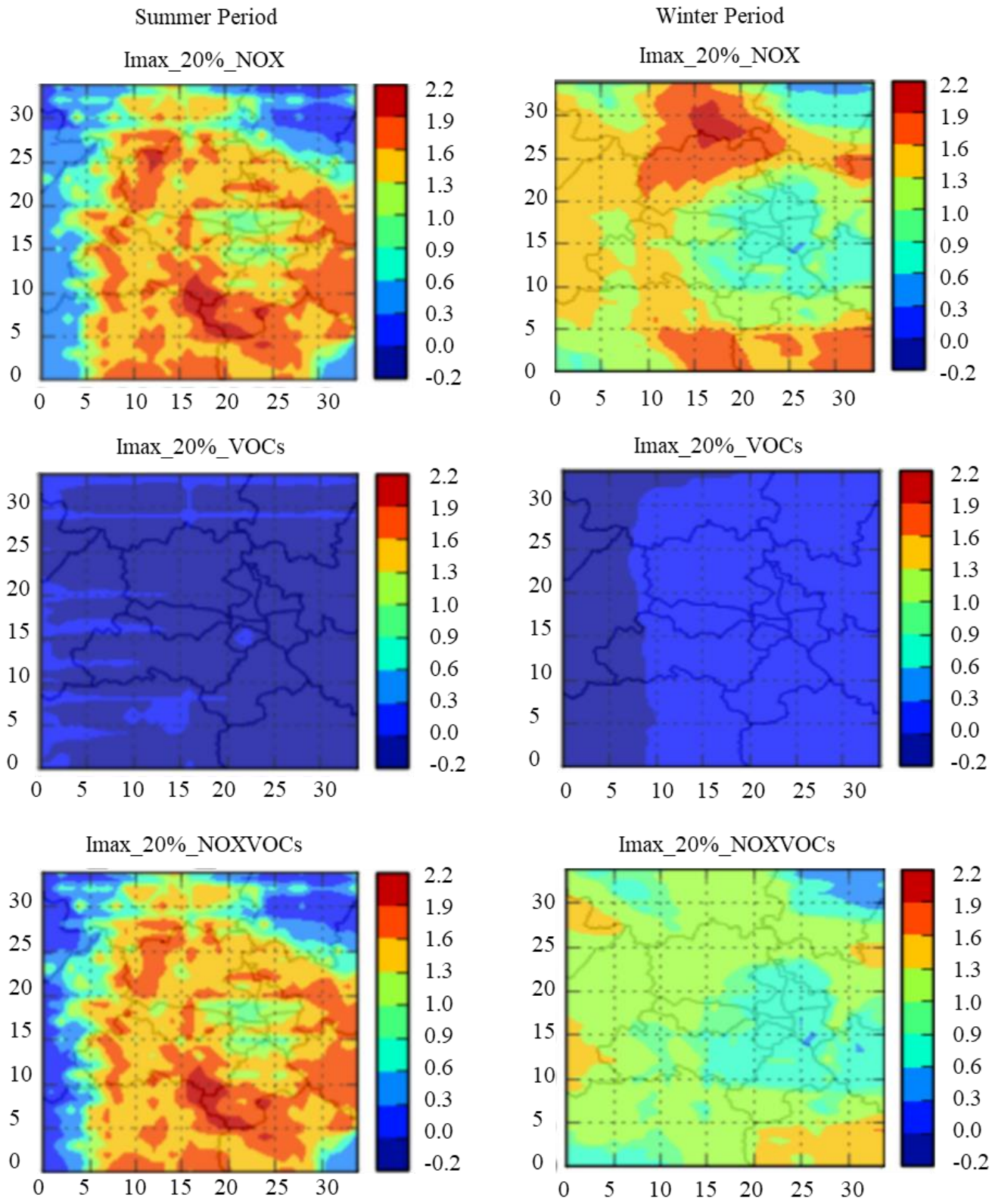

Figure-12: Maximum relative potency (Imax) as a result of the study region's summer and winter simulation periods' reduction in emissions of the major precursors of O_3 (NOX, VOCs).

Conclusion

This study reflects the importance of regional emission inventory in air quality modelling and prediction of different criteria gaseous pollutants using Polyphemus/Polair3D CTM over Delhi, India. i. The impact of regional emission inventory prepared for the base year 2010 on the simulations of gaseous species like O_3, NO_2, NO, CO and SO_2 is analyzed over the national capital of India. Regional emission inventory takes into account of various sectors such as industry, road transport, waste disposal and burning, brick kilns, vehicles etc. ii. To take into account the effect of regional emission sources on simulated gaseous species diurnal variation, time-series plots and statistical metrics are analyzed at multiple monitoring stations situated in the simulation domain. Local emission inventory is performing relatively better in comparison to EDGAR for the prediction of O_3, CO, NO_2 and SO_2 concentrations. iii. CTM Polair3D is able to capture the regional hotspots of emission sources using a local emission database. iv. In the case of global inventory except O_3, the simulated value of other gaseous pollutants NO_2, CO, and SO_2 are severely under-predicted in comparison to monitored data at various locations in the study domain. v. The differences between EDGAR and the local emission inventory, in terms of mean spatial distribution of emissions exhibit better allocation of emission sources. vi. The megacity emission estimates provide an important resource for studying future emission scenarios of the region. As the monitored data cannot be used in dynamic mode, therefore the air quality model is extremely conducive to analysing the effect of emission reductions on the concentration of different criteria pollutants. vii. Indicators like relative potency and maximum potency are extremely useful to fetch the magnitude of the effect of regional sources of emission generation in comparison to the external agent's role and also quantify the impact of different major precursors. Further work needs to improve the regional emission inventory by incorporation of various other sources of air pollutants. Improved emission inventory at finer resolution further helps in better health impact assessment of air quality in the study region.

Acknowledgment

The author thanks IIT Delhi HPC facility for computational and storage resources. The author is grateful to Yelva Roustan and Youngseob Kim from the Centre d'Enseignement et de Recherche en Environnement Atmosphérique (CEREA), France, for their assistance and support in setting up Polyphemus/Polair3D.

References

1. Guttikunda, S.K. and Calori, G. (2013). A GIS Based Emissions Inventory at 1 km x 1 km Spatial Resolution for Air Pollution Analysis in Delhi, India. *Atmos. Environ*., 67, 101–111.

2. Gurjar, B.R., van Aardenne, J.A., Lelieveld, J. and Mohan, M. (2004). Emission estimates and trends (1990–2000) for megacity Delhi and implications. *Atmos. Environ*., 38, 5663–5681.

3. Kansal, A., Khare, M and Sharma, C.S. (2011). Air quality modelling study to analyse the impact of the World Bank emission guidelines for thermal power plants in Delhi. *Atmos. Pollut. Res*., 2, 99–105.

4. Sahu, S.K., Beig, G. and Parkhi, N.S. (2011). Emissions Inventory of Anthropogenic PM2.5 and PM10 in Delhi during Commonwealth Games 2010. *Atmos. Environ*., 45, 6180–6190.

5. Nagpure, A.S., Gurjar, B.R. and Martel, J.C. (2014). Human health risks in national capital territory of Delhi due to air pollution. *Atmos. Pollut. Res*., 5(3), 371-380.

6. Daniels MJ, Dominici F, Samet JM and Zeger SL (2000). Estimating particulate matter-mortality dose-response curves and threshold levels: an analysis of daily time-series for the 20 largest US cities. *Am J Epidemiol*; 152, 397–406.

7. Dockery, D.W. and Pope, C.A. (1994). Acute Respiratory Effects of Particulate Air Pollution. *Annu. Rev. Public Health*, 15, 107-132.

8. Schwartz, J. (1994). Air Pollution and Daily Mortality: A Review and Metaanalysis. *Environ. Res*., 64, 36-52.

9. Davidson, A. (1993). Update on ozone trends in California's south coast air basin. *Air & Waste*, 43(2), 226-240.

10. Wakamatsu, S., Ohara, T. & Uno, I. (1996). Recent trends in precursor concentrations and oxidant distributions in the Tokyo and Osaka areas. *Atmospheric Environment,* 30(5), 715-721.

11. Jacob, D. J., & Winner, D. A. (2009). Effect of climate change on air quality. *Atmospheric environment*, 43(1), 51-63.

12. Oke T.R. (1995). The heat island of the urban boundary layer: characteristics, causes and effects. In: Cermak JE, Davenport AG, Plate EJ, Viegas DX (eds) Wind Climate in Cities. NATO ASI Series E: Applied Sciences - Vol. 277, Boston: Kluwer Academic Publishers, 81-108.

13. Martilli, A., Clappier, A., and Rotach, M.W. (2002). An urban surface exchange parameterization for mesoscale models. Boundary-Layer Meteorology, 104, 261-304.

14. Vautard, R., Honoré, C., Beekmann, M., and Rouil, L. (2005). Simulation of ozone during the August 2003 heat wave and emission control scenarios. *Atmos. Environ*. 39, 2957–2967.

15. Sillman, S. and Samson, P. J. (1995). Impact of temperature on oxidant photochemistry in urban, polluted rural and remote environments. *J. Geophys. Res. Atmos*., 100, 11497-11508.

16. Rubin, J. I., Kean, A. J., Harley, R. A., Millet, D. B. and Goldstein, A. H. (2006). Temperature dependence of volatile organic compound evaporative emissions from motor vehicles, J. Geophys. Res.-Atmos., 111, d03305, doi: 10.1029/2005JD006458.

17. Strassburger, A., & Kuttler, W. (1998). Diurnal courses of ozone in an inner urban park. *Meteorologische Zeitschrift*, 7.

18. Guttikunda, S. (2009). Photochemistry of air pollution in Delhi, India. *Sim air working paper series*, 25.

19. Lam, K. S., Wang, T. J., Wu, C. L., & Li, Y. S. (2005). Study on an ozone episode in hot season in Hong Kong and transboundary air pollution over Pearl River Delta region of China. *Atmospheric Environment*, 39(11), 1967-1977.

20. Chan, C. Y., Li, Y. S., Tang, J. H., Leung, Y. K., Wu, M. C., Chan, L. Y., ... & Liu, S. C. (2007). An analysis on abnormally low ozone in the upper troposphere over subtropical East Asia in spring 2004. *Atmospheric Environment*, 41(17), 3556-3564.

21. Crutzen, P. J. (1973). A discussion of the chemistry of some minor constituents in the stratosphere and troposphere. *Pageoph*., 106-108: 1385-99.

22. Crutzen, P. J. (1979). The role of NO and NO2 in the chemistry of the troposphere and stratosphere. *Ann. Rev. Earth Planet. Sci*., 7: 443-72.

23. Grell, G. A., Peckham, S. E., Schmitz, R., McKeen, S. A., Frost, G., Skamarock, W. C. and Eder, B. (2005). Fully coupled "online" chemistry within the WRF model. *Atmos. Environ*., 39, 6957–6975.

24. Zhang, Y. (2008). Online-coupled meteorology and chemistry models: history, current status, and outlook. *Atmos. Chem. Phys*., 8, 2895–2932, doi: 10.5194/acp-8-2895-2008

25. Sindhwani, R., Goyal, P., Kumar, S., & Kumar, A. (2015). Anthropogenic Emission Inventory of Criteria Air Pollutants of an Urban Agglomeration-National Capital Region (NCR), Delhi. *Aerosol and Air Quality Research*, 15(4), 1681-1697.

26. Sindhwani, R. and Goyal, P (2014). Assessment of traffic-generated gaseous and particulate matter emissions and trends over Delhi (2000−2010). *Atmos. Pollut. Res.*, 5(3), 438-446.

27. Nagpure, A.S., Sharma, K. and Gurjar, B.R. (2013). Traffic induced emission estimates and trends (2000–2005) in megacity Delhi. *Urban Climate*, 4, 61–73.

28. Kumar, A., & Goyal, P. (2011). Forecasting of daily air quality index in Delhi. *Science of the Total Environment*, 409(24), 5517-5523.

29. Mallet, V., Quélo, D., Sportisse, B., Ahmed de Biasi, M., Debry, É., Korsakissok, I., Wu, L., Roustan, Y., Sartelet, K., Tombette, M. and Foudhil, H. (2007). Technical Note: The air quality modeling system Polyphemus. *Atmos. Chem. Phys*., 7, 5479-5487.

30. Mallet, V., & Sportisse, B. (2004). 3-D chemistry-transport model Polair: numerical issues, validation and automatic-differentiation strategy. *Atmospheric Chemistry and Physics Discussions*, 4(2), 1371-1392.

31. Mallet, V and B. Sportisse (2005). A comprehensive study of ozone sensitivity with respect to emissions over Europe with a chemistry-transport model. *J. Geophys. Res.*, 110, D22302, doi: 10.1029/2005JD006234.

32. Que´lo, D., V. Mallet, and B. Sportisse (2005). Inverse modeling of NOx emissions at regional scale over northern France: Preliminary investigation of the second-order sensitivity. *J. Geophys. Res*., 110, D24310, doi: 10.1029/2005JD006151.

33. Louis, J. F. (1979). A parametric model of vertical eddy fluxes in the atmosphere. *Boundary-Layer Meteorology,* 17, 187-202.

34. Troen, I.B. and Mahrt, L., (1986). A simple model of the atmospheric boundary layer; sensitivity to surface evaporation. *Boundary-Layer Meteorology*, 37, 129-148.

35. Wesely, M.L. (1989). Parameterization of surface resistances to gaseous dry deposition in regional-scale numerical models. *Atmospheric Environment*, 23, 1293-1304.

36. Zhang, L., Gong, S., Padro, J. and Barrie, L., (2001). A size-seggregated particle dry deposition scheme for an atmospheric aerosol module. *Atmospheric Environment*, 35, 549–560.

37. Sportisse, B. and Dubois, L. (2002). Numerical and theoretical investigation of a simplified model for the parameterization of below-cloud scavenging by falling raindrops. *Atmospheric Environment*, 36, 5719-5727.

38. Zhang, L., Brook, J. and Vet, R., (2003). A revised parameterization for gaseous dry deposition in air quality models. *Atmospheric Chemistry and Physics Discussions*, 3, 2067-2082.

39. Yarwood, G., Rao, S., Yocke, M., and Whitten, G. Z. (2005). Updates to the Carbon Bond Chemical Mechanism: CB05. Tech. rep., US Environmental Protection Agency.

40. Gurjar, B. R., Van Aardenne, J. A., Lelieveld, J., & Mohan, M. (2004). Emission estimates and trends (1990–2000) for megacity Delhi and implications. *Atmospheric Environment*, 38(33), 5663-5681.

41. Energy Statistics of India (2018). http://mospi.nic.in/sites/default/files/publication_reports/Energy_Statistics_2018.pdf

42. Maithel, S., Uma, R., Bont, T., Baum, E. and Thao, V.T.K. (2012). Brick Kilns Performance Assessment, Emissions

Measurements, & a Roadmap for Cleaner Brick Production in India. Study prepared by Green Knowledge Solutions, New Delhi, India.

43. Shankar, S. (2014). Study of Air Pollution in Delhi Due to Diesel Generator Sets Used in Telecommunication. 1–42. Centre for Atmospheric Sciences, Indian Institute of Technology, Delhi, M.Tech Dissertation.

44. Emmons, L. K., Walters, S., Hess, P. G., Lamarque, J. F., Pfister, G. G., Fillmore, D., Granier, C., Guenther, A., Kinnison, D., Laepple, T., Orlando, J., Tie, X., Tyndall, G., Wiedinmyer, C., Baughcum, S. L., and Kloster, S. (2010). Description and evaluation of the Model for Ozone and Related chemical Tracers, version 4 (MOZART-4). *Geosci. Model Dev*., 3, 43-67, doi: 10.5194/gmd-3-43-2010.

45. Verwer, J. G., Hundsdorfer, W., and Blom, J. G. (1998): Numerical time integration for air pollution models. technical report, CWI.

46. Verwer, J. G., Spee, E. J. Blom, J. G. and Hundsdorfer, W (1999). A second-order Rosenbrock method applied to photochemical dispersion problems. SIAM J. Sci. Comput., 20, 1456–1480.

47. Chen, F. and Dudhia, J. (2001). Coupling an advanced land- surface/hydrology model with the Penn State/NCAR MM5 modeling system. Part I: Model description and implementation, *Mon. Weather Rev.,* 129, 569–585.

48. Mlawer, E. J., Taubman, S. J., Brown, P. D., Iacono, M. J., and Clough, S. A. (1997). Radiative transfer for inhomogeneous atmosphere: RRTM, a validated correlated-k model for longwave. *J. Geophys. Res*., 102(D14), 16663–16682.

49. Lin, Y. L., R. D. Farley, and H. D. Orville (1983). Bulk parameterization of the snow field in a cloud model. *J. Clim. Appl. Meteorol*., 22, 1065–1092, doi: 10.1175/1520-0450(1983)022<1065:BPOTSF>2.0.CO; 2.

50. Hong, S.Y., Noh, Y. and Dudhia, J. (2006). A new vertical diffusion pack- age with an explicit treatment of entrainment processes. *Mon. Weather Rev.*, 134, 2318–2341.

51. Chou, M. D. and Suarez, M. J. (1994). An efficient thermal infrared radiation parameterization for use in general circulation models. *NASA Tech. Memo*. 104606, 85.

52. Stockwell, W.R., Middleton, P., Chang, J.S. and Tang, X., (1990). second-generation regional acid deposition model chemical mechanism for regional air quality modeling. *Journal of Geophysical Research*, 95, 16343–16367.

53. Stockwell, W.R., Kirchner, F., Kuhn, M. and Seefeld, S., (1997). A new mechanism for regional atmospheric chemistry modeling. *Journal of Geophysical Research*, 102, 25847–25879.

54. Wild, O., Zhu, X., and Prather, M. J. (2000). Fast-J: Accurate simulation of in and below cloud photolysis in tropospheric chemical models. *J. Atmos. Chem*., 37, 245–282.

55. Monin, A. S., and Obukhov, A. M. (1954). Basic laws of turbulent mixing in the surface layer of the atmosphere. *Tr. Akad. Nauk SSSR Geofiz. Inst*., 24, 163–187.

56. Kain, J.S. (2004). The Kain–Fritsch convective parameterization: an update. *Journal of Applied Meteorology*, 43, 170–181.

57. G. Janssens-Maenhout et al. (2011). EDGAR-HTAP: a harmonized gridded air pollution emission dataset based on national inventories. doi:10.2788/14102.

58. De Meij, A., Krol, M., Dentener, F., Vignati, E., Cuvelier, C. and Thunis, P (2006). The sensitivity of aerosol in Europe to two different emission inventories and temporal distribution of emissions. *Atmos. Chem. Phys.* 6, 4287–4309.

59. Pregger, T. and Friedrich, R. (2009). Effective pollutant emission heights for atmospheric transport modelling based on real-world information. *Environ. Poll*., 157, 552–560, doi:10.1016/j.envpol.2008.09.027.

60. Thunis, P. and Clappier, A. (2014). Indicators to support the dynamic evaluation of air quality models. *Atmos. Environ*., 98, 402-409.

61. Seinfeld, J. and Pandis, S. (1998). Atmospheric chemistry and physics: From air pollution to climate change (2nd ed.). Hoboken, New Jersey: Wiley.

62. Seinfeld, J.H. (1989). Urban air pollution: State of science. *Science*, 243, 745-753.

63. Logan, J.A., M.J. Prather, S.C. Wofsy and M.B. McElroy (1981). Tropospheric chemistry: A global perspective. *J. Geophys. Res*., 86, 7210-7254.

64. Brewer, D.A., T.R. Augustsson, and J.S. Levine. (1983). The photochemistry of anthropogenic nonmethane hydrocarbons in the troposphere. *J. Geophys. Res.,* 88, 6683-6695.

65. Finlayson-Pitts, B.J. and J.N. Pitts, Jr. (1986). Atmospheric Chemistry: Fundamentals and Experimental Techniques. New York: Wiley-Inter science Publication. 1098pp.

66. Sillman, S., J. A. Logan, and S. C. Wofsy (1990). The sensitivity of ozone to nitrogen oxides and hydrocarbons in regional ozone episodes. *J. Geophys. Res*., 95(D2), 1837-1851. doi:10.1029/JD095iD02p01837.

67. Folberth, G.A., Rumbold, S.T., Collins, W.J. and Butler, T.M. (2012). Global radiative forcing and megacities. *Urban Clim*. 1 (2012), 4–19.

68. Mena-Carrasco, M., Carmichael, G.R., Campbell, J.E., Zimmerman, D., Tang, Y., Adhikary, B., D'allura, A., Molina, L.T., Zavala, M., García, A., Flocke, F., Campos, T., Weinheimer, A.J., Shetter, R., Apel, E., Montzka, D.D., Knapp, D.J., Zheng, W., (2009). Assessing the regional

impacts of Mexico City emissions on air quality and chemistry. *Atmos. Chem. Phys*., 9, 3731–3743. http:// dx.doi.org/10.5194/acp-9-3731-2009.

69. Tarrason L., Jonson J.E., Fagerli H., Benedictow A., Wind P., Simpson D. and Klein H., (2003). Transboundary Acidification, Eutrophication and Ground Level Ozone in Europe, Part III. Source-receptor relationships, 2003. EMEP MSC-W Report 1/ 2003, Norwegian Meteorological Institute, Oslo, Norway.

70. deMeij, A., Thunis, P., Bessagnet, B. and Cuvelier, C. (2009). The sensitivity of the CHIMERE model to emissions reduction scenarios on air quality in Northern Italy. *Atmos. Environ*. 43, 1897–1907.

71. Finardi, S., Silibello, C., D'Allura, A., & Radice, P. (2014). Analysis of pollutants exchange between the Po Valley and the surrounding European region. *Urban Climate*, 10, 682-702.

72. Guttikunda, S.K., Tang, Y., Carmichael, G.R., Kurata, G., Pan, L., Streets, D.G., Woo, J.-H., Thongboonchoo, N., Fried, A., (2005). Impacts of Asian megacity emissions on regional air quality during spring 2001. *J. Geophys. Res.,* 110, D20301. http://dx.doi.org/10.1029/2004JD004921